Editors' Suggestion

Microscopic Origin of Frictional Rheology in Dense Suspensions: Correlations in Force Space

Jetin E. Thomas,[1,*] Kabir Ramola,[1,†] Abhinendra Singh,[2,‡] Romain Mari,[3,§] Jeffrey F. Morris,[2,4,¶] and Bulbul Chakraborty[1,**]

[1]*Martin Fisher School of Physics, Brandeis University, Waltham, Massachusetts 02454, USA*
[2]*Benjamin Levich Institute, CUNY City College of New York, New York, New York 10031, USA*
[3]*Université Grenoble Alpes, CNRS, LIPhy, 38000 Grenoble, France*
[4]*Department of Chemical Engineering, CUNY City College of New York, New York, New York 10031, USA*

(Received 6 April 2018; revised manuscript received 26 July 2018; published 21 September 2018)

We develop a statistical framework for the rheology of dense, non-Brownian suspensions, based on correlations in a space representing forces, which is dual to position space. Working with the ensemble of steady state configurations obtained from simulations of suspensions in two dimensions, we find that the anisotropy of the pair correlation function in force space changes with confining shear stress (σ_{xy}) and packing fraction (ϕ). Using these microscopic correlations, we build a statistical theory for the macroscopic friction coefficient: the anisotropy of the stress tensor, $\mu = \sigma_{xy}/P$. We find that μ decreases (i) as ϕ is increased and (ii) as σ_{xy} is increased. Using a new constitutive relation between μ and viscosity for dense suspensions that generalizes the rate-independent one, we show that our theory predicts a discontinuous shear thickening flow diagram that is in good agreement with numerical simulations, and the qualitative features of μ that lead to the generic flow diagram of a discontinuous shear thickening fluid observed in experiments.

DOI: 10.1103/PhysRevLett.121.128002

Dense suspensions of frictional grains in a fluid often display an increase in viscosity $\eta = \sigma_{xy}/\dot{\gamma}$ (thickening) as the confining shear stress (σ_{xy}) or strain rate ($\dot{\gamma}$) are increased. At a critical density-dependent shear rate $\dot{\gamma}$, the viscosity increases abruptly: a phenomenon termed discontinuous shear thickening (DST). In stress-controlled protocols, $\eta \sim \sigma_{xy}$ marks the DST boundary [1,2]. Experiments have also observed interesting features in other components of the stress tensor such as the first normal stress difference, $N_1 = \sigma_{xx} - \sigma_{yy}$ close to the DST regime [3]. A mean-field theory [4,5], based on an increase in the fraction of close interactions becoming frictional (rather than lubricated) with increasing shear stress, has been extremely successful at predicting the flow curves and the DST flow diagram in the space of packing fraction ϕ and shear stress or strain rate [6,7]. The physical picture of lubricated layers between grains giving way to frictional contacts when the imposed σ_{xy} exceeds a critical value set by a repulsive force [4] provides a consistent theory of DST [7], shear-jamming fronts [8], and instabilities of the shear-thickened state [9].

Although several features relating to the flow of dense suspensions can be well explained within this mean-field theory, the nature of the microscopic correlations underlying this transition remains far from clear [6]. Conventional measures such as the pair correlation function do not exhibit pronounced changes accompanying DST. An interesting, intrinsic feature of DST is that the macroscopic friction coefficient μ *decreases* as the fraction of frictional contacts *increases*: the mean normal stress grows more rapidly than the shear stress. This, and contact network visualizations from simulations [6], indicate that there are important changes in the network of frictional contacts that are not captured by scalar variables such as the fraction of frictional contacts. In this work, we focus on the microscopic origin of the evolution of the components of the stress tensor across DST and construct a statistical theory for μ, the anisotropy of the stress tensor.

While the changes in real space near DST can be incremental, and hence do not show any significant changes in pair correlations, the contact forces change dramatically and play a central role. The steady state flow of noninertial suspensions is governed by microscopic constraints of force and torque balance, and these constraints can lead to nontrivial correlations of contact forces. Theories have focused, up to now, on the *average* properties of the interparticle forces [4]. However, fundamental questions about how interactions at the microscopic, contact level and the constraints of force balance give rise to a macroscopic transition remain [10].

In two-dimensional systems, the crucial constraint of force balance can be naturally accounted for by working in a *dual* space, known as a force tiling. In this representation, interparticle forces are represented by the difference of

vector *height fields* $\{\vec{h}\}$ defined on the voids. This representation has been shown to be particularly useful in characterizing shear-jamming transitions in frictional granular materials [11]. Unlike shear jamming, where configurations and stresses are static, flowing suspensions provide an *ensemble* of nonequilibrium steady states (NESS) that are ripe for a statistical description. We show that the nonequilibrium steady states at a given σ_{xy} and ϕ can be mapped to a statistical ensemble characterized by an *a priori* probability distribution. This distribution is constructed from the measured pair correlation functions in force space.

In the continuum, the height fields define the local Cauchy stress tensor, by the relation $\overleftrightarrow{\sigma} = \nabla \times \vec{h}$, and the area integral of $\overleftrightarrow{\sigma}$, or the force moment tensor $\overleftrightarrow{\Sigma}$ [12], in terms of difference of the height fields across the system:

$$\overleftrightarrow{\sigma} = \begin{pmatrix} \partial_y h_x & \partial_y h_y \\ -\partial_x h_x & -\partial_x h_y \end{pmatrix}, \qquad \overleftrightarrow{\Sigma} = \begin{pmatrix} L_y \Gamma_{yx} & L_y \Gamma_{yy} \\ -L_x \Gamma_{xx} & -L_x \Gamma_{xy} \end{pmatrix}, \tag{1}$$

where $\vec{\Gamma}_{x(y)}$ represents the sum of forces along the $x(y)$ directions, and $L_{x(y)}$ represents the linear dimensions of the system ($\overleftrightarrow{\sigma} = \overleftrightarrow{\Sigma}/L_x L_y$). Additionally, global torque balance implies $\Sigma_{xy} = \Sigma_{yx}$. In our simulations $L_x = L_y = L$; hence, $\Gamma_{yy} = -\Gamma_{xx} = L\sigma_{xy} = \sigma$. Working with the ensemble of force tilings generated from the NESS created in simulations, we observe changes in the anisotropy of the pair correlation function of the vertices (PCFV) of the tilings as ϕ and σ_{xy} are changed. Using these microscopic correlations, we build a statistical theory for $\overleftrightarrow{\Sigma}$. The reason for using the components of $\overleftrightarrow{\Sigma}$ is their clear geometric signatures in the force tilings, as shown in Fig. 1. The stress anisotropy is defined as the ratio of the difference in eigenvalues τ to the trace $2P = \sigma_{xx} + \sigma_{yy}$ of $\overleftrightarrow{\sigma}$, which can also be related to the components of $\overleftrightarrow{\Sigma}$:

$$\frac{\tau}{2P} = \frac{\sqrt{\tilde{N}_1^2 + 4\Sigma_{xy}^2}}{\Sigma_{xx} + \Sigma_{yy}}, \tag{2}$$

where $\tilde{N}_1 = \Sigma_{xx} - \Sigma_{yy}$. In the limit of $\tilde{N}_1 \to 0$, $\tau/2P$ is identical to the macroscopic friction coefficient $\mu = \sigma_{xy}/P$. In this Letter, we show that the change in the macroscopic friction coefficient $\mu(\phi, \sigma_{xy})$ across the DST transition [13] can be obtained from a statistical theory based on an effective pair potential between the vertices of the force tilings. An extension of the quasi-Newtonian, rate-independent, suspension rheology model [22,23] can then be used to compute the viscosity $\eta(\phi, \sigma_{xy})$:

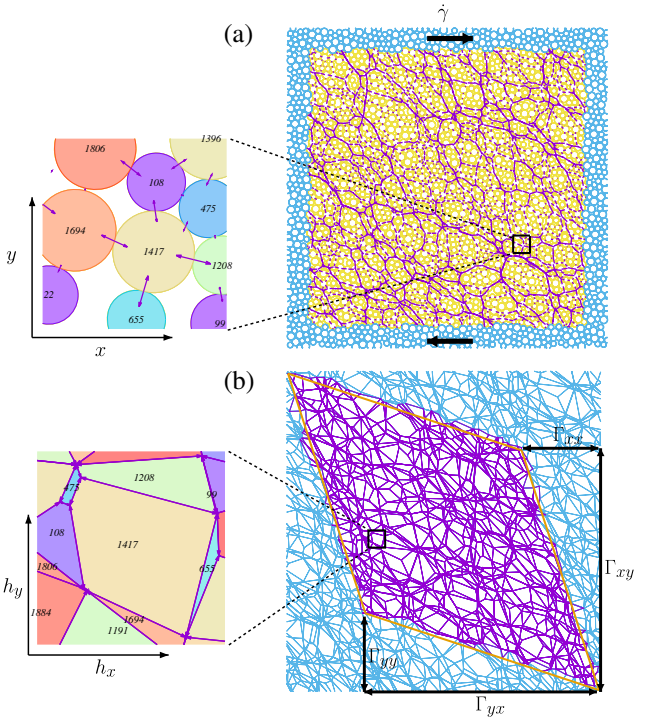

FIG. 1. (a) A snapshot of a sheared suspension of 2000 soft frictional disks. The lines represent the pairwise (lubricated and frictional contact) force vectors between the individual grains. (b) The force tiling associated with this flowing dense suspension. The bonds correspond to the pairwise forces, with larger polygons representing grains with higher stress. The vertices of the tiling represent height vectors $\vec{h} = (h_x, h_y)$, whose difference provides the pairwise force at each bond. $\vec{\Gamma}_x = (\Gamma_{xx}, \Gamma_{xy})$ and $\vec{\Gamma}_y = (\Gamma_{yx}, \Gamma_{yy})$ represent the sum of forces in the x and y directions, respectively. The light blue regions represent periodic copies of the system.

$$\eta(\phi, \sigma_{xy}) \propto \mu(\phi, \sigma_{xy})[\mu(\phi, \sigma_{xy}) - \mu_c]^{-2}. \tag{3}$$

As we show [13], this constitutive relation is valid for thickening suspensions in the limit of $\phi \to \phi_m^-$, where ϕ_m is the frictional jamming point. We use our microscopic theory of μ in conjunction with this constitutive relation to predict the rheological properties characterizing DST.

Simulating dense suspensions.—We perform simulations of simple shear under constant stress of a monolayer of $N = 2000$ bidisperse (radii a and $1.4a$) spherical particles by methods described in detail previously [6]. These follow an overdamped dynamics and are subject to Stokes drag, pairwise lubrication, frictional contact, and short-range repulsive forces (see Supplemental Material [13]). Because of the repulsive force of maximum F_0 at contact, frictional contacts only form for stresses about or larger than $\sigma_0 \equiv F_0/a^2$, which induces DST at volume fractions $\phi \gtrsim 0.78$ [6].

Force space representation.—For a force balanced configuration of grains with pairwise forces, the "vector

sum" of forces on every grain, i.e., the force vectors arranged head to tail (with a cyclic convention), form a *closed polygon*. Next, Newton's third law imposes the condition that every force vector in the system has an equal and opposite counterpart that belongs to its neighboring grain. This leads to the force polygons being exactly edge matching. Extending this to all particles within the system leads to a "force tiling" [11,24]. The adjacency of the faces in the tiling is the adjacency of the grains, whereas the adjacency of the vertices is the adjacency of the voids (the heights are associated with the voids in the network). In addition to the pairwise forces between grains, each particle experiences a hydrodynamic drag, which can be represented as a *body force*. Imposing the constraints of vectorial force balance in the presence of body forces leads to a unique solution for modified height fields, given the geometrical properties of the contact network [25]. This allows us to construct the ensemble of force tilings corresponding to the NESS of the suspension. The distribution of the hydrodynamic drag force to contacts through the modified height vectors leads to some very small contact forces that do not represent "real contacts." As we discuss below, we have a systematic way of neglecting these in our statistical analysis.

Pair correlation functions.—Using the force tiling representation, we compute the PCFV, defined to be

$$g_2(\vec{h}) = \left\langle \frac{A}{N_v(N_v-1)} \sum_{i=1}^{N_v} \sum_{j\neq i}^{N_v} \delta(\vec{h} - (\vec{h}_i - \vec{h}_j)) \right\rangle, \quad (4)$$

where N_v is the total number of voids in the system, $A = |\vec{\Gamma}_x \times \vec{\Gamma}_y|$, and $\rho_v = N_v/A$ is the density of height vertices in the force tiling. The PCFV are averaged over 200 configurations obtained from the simulated steady state of dense suspensions at each ϕ and σ_{xy} [13]. We find a distinct fourfold anisotropic structure in $g_2(\vec{h})$, which quantitatively captures the details of the changes in the organization of the forces acting between particles as ϕ is increased (Fig. 2). The anisotropy is sensitive, to a lesser extent, to increases in σ_{xy}. The regions where $g_2(\vec{h}) < 1$ indicate regions of larger contact forces, statistically, since this is where the height vertices are farther apart than expected for an uncorrelated distribution. As seen from Fig. 2, these regions lie along the compressive direction for all values of ϕ and σ_{xy}. Complementing these are the regions with $g_2(\vec{h}) > 1$, which indicate regions of smaller forces. The angles between these regions clearly increase as ϕ increases [13]. These changes in $g_2(\vec{h})$, especially its anisotropy, have important consequences for the stress tensor, as we show below.

Statistical ensemble.—Each force tiling is specified by a set of vertices and a set of edges that connect these vertices. The distances between the vertices quantify the internal stress in the system, whereas the edges, which quantify the specific contact forces in a configuration, can be thought of, in a statistical sense, as fluctuating quantities, with connections between pairs of vertices chosen with some weights. We thus treat these vertices of the force tilings as the points of an interacting system of particles. These effective interactions arise from the constraints of mechanical equilibrium, and from integrating out the edges. We represent this effective interaction by a noncentral potential computed from the measured pair correlation function, similar to constructions used in colloidal and polymer theory [26]:

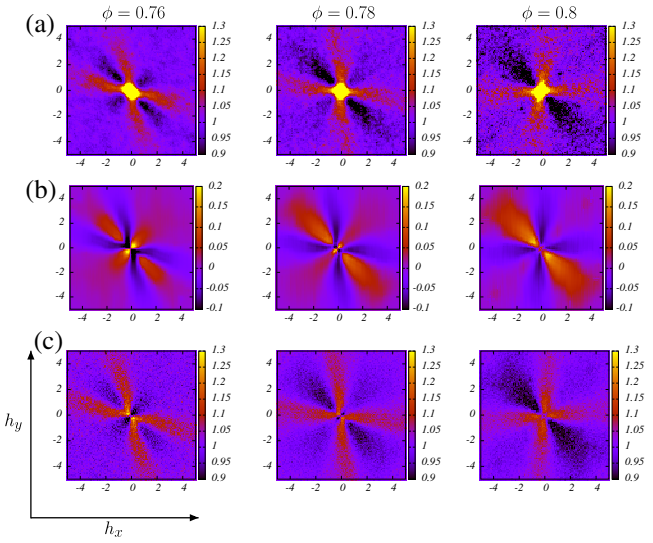

FIG. 2. (a) Observed pair correlation functions at $\sigma_{xy} = 2\sigma_0$, at packing fractions $\phi = 0.76$, 0.78, and 0.8. $\phi = 0.8$ is above ϕ_{DST}: the onset packing fraction for a regime of stress over which the viscosity scales as σ, which defines DST (see Ref. [13]). The forces (and consequently the heights) have been scaled by the imposed shear stress. The change in symmetry of $g_2(\vec{h})$ is clearly visible as the packing fraction is increased. (b) Potentials constructed using these pair correlation functions [Eq. (5)]. (c) A comparison with pair correlations obtained from direct Monte Carlo simulations of particles interacting via these potentials.

$$V_2(\vec{h}) = -\log\left(\frac{g_2(\vec{h})}{g_2(|\vec{h}|)}\right). \quad (5)$$

The regularization through division by $g_2(|\vec{h}|)$ is necessary because there is strong clustering at very small distances in height space [13], which reflects the behavior of very small forces, much smaller than the repulsive force that needs to be overcome to create frictional contacts [6,13]. In addition, we add a short-ranged repulsive potential to $V_2(\vec{h})$ that prevents clustering of vertices at the smallest force scales [13]. The resulting potential $V_{\phi,\sigma}(\vec{h})$ thus represents interactions at intermediate and large scales in the force tilings.

This potential encodes the full anisotropy of $g_2(\vec{h})$, and as we show below, this is crucial for understanding the evolution of the anisotropy of the stress tensor. To check whether such a potential is successfully able to reproduce the original correlations, we perform Monte Carlo simulations, as described in detail in Ref. [13]. The $g_2(\vec{h})$ obtained from the Monte Carlo simulations are shown in Fig. 2, and demonstrate that $V_2(\vec{h})$ captures the properties at all but the smallest force scales.

The force tiles obtained from the simulations form an ensemble with microstates defined by the set $\mathcal{C} \equiv \{\vec{h}_i\}$. The fundamental assumption we make is that this ensemble of NESS is characterized by an *a priori* probability $p(\mathcal{C}) \propto \exp[-V(\mathcal{C})]$, where $V(\mathcal{C}) = \sum_{i,j\neq i} V_{\phi,\sigma}(\vec{h}_i - \vec{h}_j)$ is the analog of the total energy of a configuration in equilibrium statistical mechanics. We then characterize the properties of the NESS by this generalized statistical ensemble. The partition function of the system is then

$$Z_{\phi,\sigma} = \frac{1}{N_v!}\int_0^\infty dA \exp\left(-N_v f_p^* A\right) \times \underbrace{\int_A \prod_{i=1}^{N_v} d\vec{h}_i \exp\left(-\sum_{i,j} V_{\phi,\sigma}(\vec{h}_i - \vec{h}_j)\right)}_{A^{N_v}\exp[-\epsilon_{\phi,\sigma}(A,N_v)]} = \int_0^\infty dA \exp(-\mathcal{F}_{A;\phi,\sigma}), \tag{6}$$

where the positions $\vec{h}_i$ are confined to be within the box with area A, which is related to stresses since this is the area of the *force tiling*. Here, f_p^* plays the role of a pressure in the "*NPT*" ensemble in equilibrium statistical mechanics of particles, and controls the fluctuations of A. Since N_1 is observed to be small in the simulations, we assume that it vanishes, which leads to the relationship $A = \sigma^2(1/\mu^2 - 1)$ [13].

We next construct a mean-field theory of μ by minimizing the effective "free-energy" function, $\mathcal{F}_{A;\phi,\sigma}$, referred to in the following as $\mathcal{F}$. In order to compute $\mathcal{F}$, we sample $\epsilon_{\phi,\sigma}(A, N_v)$ [Eq. (6)]. Details of the sampling method are provided in Ref. [13]. Transforming from A to μ, the free energy per vertex is given by

$$f(\mu;\phi,\sigma) \equiv \mathcal{F}/N_v = f_p^*\sigma^2\left(\frac{1}{\mu^2} - 1\right) - \log\left[\sigma^2\left(\frac{1}{\mu^2} - 1\right)\right] + \frac{\epsilon_{\phi,\sigma}(\mu, N_v)}{N_v}. \tag{7}$$

As an example, the functions $f(\mu;\phi,\sigma)$ obtained at imposed stress $\sigma_{xy} = 100\sigma_0$ at different packing fractions are shown in the inset of Fig. 3. We fix $f_p^* = 6.5 \times 10^{-4}$ to reproduce the observed value of μ at $\phi = 0.8$ and $\sigma_{xy} = 100\sigma_0$.

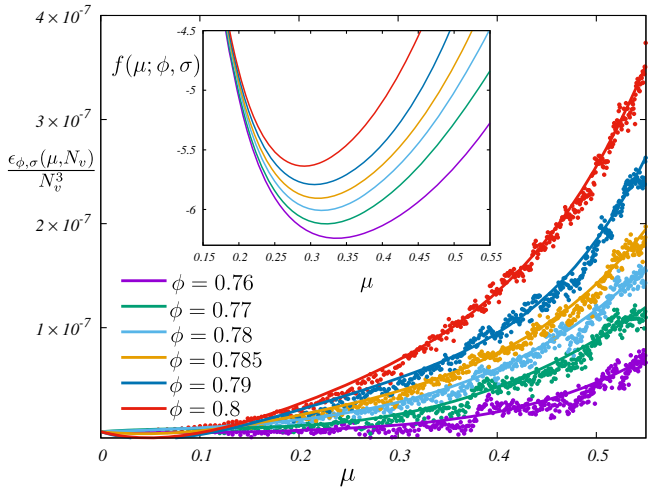

FIG. 3. Sampled values of $\epsilon_{\phi,\sigma}(\mu, N_v)$ for $N_v = 1024$ and $\sigma_{xy}/\sigma_0 = 100$, with V_2 derived from simulations at different packing fractions ϕ [Eq. (5)]. Inset: $f(\mu;\phi,\sigma)$ for $N_v = 3000$, and $f_p^* = 6.5 \times 10^{-4}$. The minimum of $f(\mu;\phi,\sigma)$ provides the value of μ at each (ϕ,σ).

Phase diagram for DST.—Finally, minimizing $f(\mu;\phi,\sigma)$, we compute $\mu(\phi,\sigma) \equiv \mu(\phi,\sigma_{xy})$, and deduce the viscosity and the DST phase diagram. The variation of μ is provided in Fig. 4. We find that μ decreases as the packing fraction ϕ and the confining shear stress σ_{xy} are increased, in agreement with the variation observed directly in the simulations [13]. Unfortunately, there are no experimental measurements of $\mu(\phi,\sigma)$ in DST suspensions. However, insight may be gained from three-dimensional

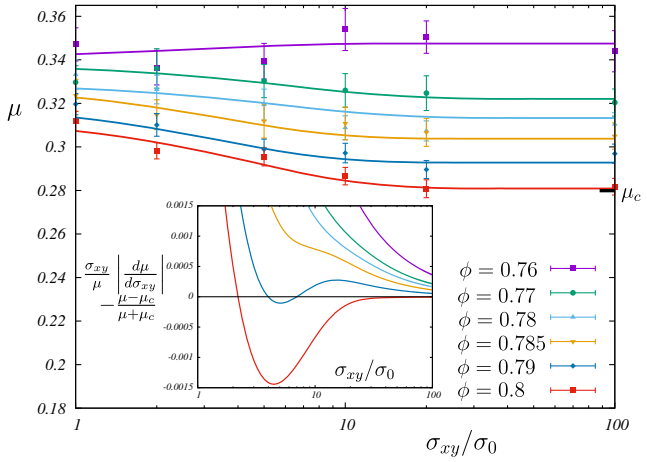

FIG. 4. Variation of the macroscopic friction coefficient μ, corresponding to the minimum of the free-energy function in Eq. (7). We find that μ decreases as packing fraction ϕ and the confining shear stress σ_{xy} are increased. Inset: Plot of Eq. (8) showing the appearance of two solutions at $\phi = 0.79$, and the second solution moving out to $\sigma_{xy} \to \infty$ at $\phi = 0.8$.

simulations of nonthickening suspensions where the second normal stress difference N_2 is found to be roughly linear with P [27], and thus the behavior of N_2 gives a reasonable approximation of that of P. In particular, Cwalina and Wagner [28] provide N_2 which is largely in agreement with the present simulation method [29]. By the present simulation method applied to three-dimensional suspensions, N_2/σ_{xy} increases (i.e., the "friction coefficient" of σ_{xy}/N_2 decreases) at DST, as seen in Fig. 6 of Ref. [6], and thus it appears reasonable that the experimental ratio of σ_{xy}/P also decreases at this transition.

The DST boundary [13] is defined by the condition $(d\dot{\gamma}/d\sigma_{xy}) = 0$. This relationship can be translated to one in terms of μ using Eq. (3):

$$\frac{\sigma_{xy}}{\mu}\left|\frac{d\mu}{d\sigma_{xy}}\right| = \frac{\mu-\mu_c}{\mu+\mu_c}. \tag{8}$$

Using the values of $\mu(\phi,\sigma)$ obtained by minimizing $f(\mu;\phi,\sigma)$, we find that Eq. (8) is satisfied at two values of the shear stress for $0.785 \leq \phi \leq 0.8$ if we choose μ_c to be $\mu(0.8, 100)$ (Fig. 4). This choice implies that the viscosity diverges at $\phi = 0.8$ in the limit of large σ, where all contacts are frictional. The inset of Fig. 4 demarcates the DST region obtained from solving Eq. (8). This region is not sensitive to the choice of μ_c as long as it is in the vicinity of the smallest value observed at $\phi \simeq 0.8$. The precise numerical values are not crucial as Eq. (8) will have two solutions as long as the generic features in $g_2(\vec{h})$ that we obtain from the simulations are preserved. The results for η as a function of ϕ and σ_{xy} are shown in Ref. [13].

Conclusion and outlook.—We have identified a correlation function that exhibits significant changes in anisotropy across the DST transition. The correlations are in force space, and reflect the collective behavior triggered by changes in the nature of the *contact forces*, which often arise due to small changes in grain positions that are difficult to identify in any positional correlations. Remarkably, a theory based on pair potentials in force space describes the macroscopic rheology. Our work also highlights the changes in the macroscopic friction coefficient, accompanying the DST transition. The decrease in μ indicates that the pressure increase for an imposed increase of shear stress is larger in the frictional branch of DST than it is in the frictionless branch of DST [23]. There is, however, no singular change in μ across the DST transition. A decrease in $\mu(\phi,\sigma)$ has also been associated with the shear-jamming transition in dry grains [30]. In that system, overlap order parameters of the force tile vertices, evocative of spin glass order parameters, characterized shear jamming [30]. In the DST steady states, these overlap parameters correspond to autocorrelation functions of the vertices of force tiles. In the future, we plan to use our statistical ensemble to relate these autocorrelation functions to changes in viscosity accompanying the DST transition. Note that in equilibrium, stress autocorrelations are related to the viscosity through the Green-Kubo relations.

The work of J. E. T., K. R., and B. C. has been supported by NSF-CBET Grant No. 1605428, NSF-DMR Grant No. 1409093, and the W. M. Keck Foundation. A. S. and J. F. M. are supported under NSF-CBET Grant No. 1605283. This research was also supported in part by the National Science Foundation under Grant No. NSF PHY11-25915. We acknowledge the hospitality of the Kavli Institute for Theoretical Physics where part of this work was carried out.

*jethomas@brandeis.edu
†kramola@brandeis.edu
‡abhinendra@uchicago.edu
§romain.mari@univ-grenoble-alpes.fr
¶morris@ccny.cuny.edu
**bulbul@brandeis.edu

[1] J. Mewis and N. J. Wagner, *Colloidal Suspension Rheology* (Cambridge University Press, Cambridge, England, 2012).
[2] E. Brown and H. M. Jaeger, Rep. Prog. Phys. **77**, 046602 (2014).
[3] J. R. Royer, D. L. Blair, and S. D. Hudson, Phys. Rev. Lett. **116**, 188301 (2016).
[4] M. Wyart and M. E. Cates, Phys. Rev. Lett. **112**, 098302 (2014).
[5] M. E. Cates and M. Wyart, Rheol. Acta **53**, 755 (2014).
[6] R. Mari, R. Seto, J. F. Morris, and M. M. Denn, J. Rheol. **58**, 1693 (2014).
[7] A. Singh, R. Mari, M. M. Denn, and J. F. Morris, J. Rheol. **62**, 457 (2018).
[8] E. Han, M. Wyart, I. R. Peters, and H. M. Jaeger, Phys. Rev. Fluids **3**, 073301 (2018).
[9] M. Hermes, B. M. Guy, W. C. Poon, G. Poy, M. E. Cates, and M. Wyart, J. Rheol. **60**, 905 (2016).
[10] S. Sarkar, E. Shatoff, K. Ramola, R. Mari, J. Morris, and B. Chakraborty, in *EPJ Web of Conferences* (EDP Sciences, 2017), Vol. 140, p. 09045.
[11] S. Sarkar, D. Bi, J. Zhang, R. P. Behringer, and B. Chakraborty, Phys. Rev. Lett. **111**, 068301 (2013).
[12] S. Henkes and B. Chakraborty, Phys. Rev. E **79**, 061301 (2009).
[13] See Supplemental Material at http://link.aps.org/supplemental/10.1103/PhysRevLett.121.128002 for details, which includes Refs. [14–21].
[14] A. Singh, J. F. Morris, and M. M. Denn, in *EPJ Web of Conferences* (EDP Sciences, 2017), p. 09023.
[15] R. Mari, R. Seto, J. F. Morris, and M. M. Denn, Phys. Rev. E **91**, 052302 (2015).
[16] H. M. Laun, J. Non-Newtonian Fluid Mech. **54**, 87 (1994).
[17] P. A. Cundall and O. D. L. Strack, Geotechnique **29**, 47 (1979).
[18] H. Herrmann and S. Luding, Continuum Mech. Thermodyn. **10**, 189 (1998).
[19] A. Singh, V. Magnanimo, K. Saitoh, and S. Luding, New J. Phys. **17**, 043028 (2015).
[20] A. Z. Panagiotopoulos, Mol. Phys. **61**, 813 (1987).

[21] S. Yashonath and C. Rao, Mol. Phys. **54**, 245 (1985).
[22] F. Boyer, É. Guazzelli, and O. Pouliquen, Phys. Rev. Lett. **107**, 188301 (2011).
[23] J. Dong and M. Trulsson, Phys. Rev. Fluids **2**, 081301 (2017).
[24] B. P. Tighe, A. R. T. van Eerd, and T. J. H. Vlugt, Phys. Rev. Lett. **100**, 238001 (2008).
[25] K. Ramola and B. Chakraborty, J. Stat. Phys. **169**, 1 (2017).
[26] P. Bolhuis, A. Louis, J. Hansen, and E. Meijer, J. Chem. Phys. **114**, 4296 (2001).
[27] Y. Yurkovetsky and J. F. Morris, J. Rheol. **52**, 141 (2008).
[28] C. D. Cwalina and N. J. Wagner, J. Rheol. **58**, 949 (2014).
[29] R. Mari, R. Seto, J. F. Morris, and M. M. Denn, Proc. Natl. Acad. Sci. U.S.A. **112**, 15326 (2015).
[30] S. Sarkar, D. Bi, J. Zhang, J. Ren, R. P. Behringer, and B. Chakraborty, Phys. Rev. E **93**, 042901 (2016).